Orbital Dynamics of an Oscillating Sail in the Earth-Moon System

By Jeannette HEILIGERS[1)] and Matteo CERIOTTI[2)]

[1)] *Faculty of Aerospace Engineering, Delft University of Technology, Delft, The Netherlands &*
Colorado Center for Astrodynamics Research, Department of Aerospace Engineering Sciences, University of Colorado Boulder, Boulder, Colorado, USA
[2)] *Systems Power and Energy, School of Engineering, University of Glasgow, Glasgow, United Kingdom*

(Received 1st Dec, 2016)

The oscillating sail is a novel solar sail configuration where a triangular sail is released at a deflected angle with respect to the Sun-direction. As a result, the sail will conduct an undamped oscillating motion around the Sun-line due to the offset between the centre-of-pressure and centre-of-mass. In this paper, the resulting oscillatory motion of the acceleration vector is exploited to design new families of periodic orbits in the Earth-Moon circular restricted three-body system. In particular, the effect of adding an oscillating sail to the family of Lyapunov orbits at the L_1- and L_2-points as well as the family of distant retrograde orbits (DROs) is investigated. Because the solar sail Earth-Moon system is non-autonomous (due to the apparent orbital motion of the Sun), the sail's oscillating period, the orbital period and the period of the Sun around the Earth-Moon system all need to be commensurable in order for the orbits to be repeatable over time. Using a differential correction technique, orbits that satisfy these constraints can be obtained and the results comprise new families of periodic orbits that are parameterised by the required sail performance. In addition to exploiting the oscillating sail for generating new orbit families, this paper also investigates its potential for orbital transfers. By combining a systematic search method with a local optimiser, oscillating sail parameters and orbital parameters can be obtained that enable transfers between classical Lyapunov orbits at the L_1-point, connections between classical Lyapunov orbits at different Lagrange points as well as transfers between orbits within the family of classical DROs.

Key Words: Solar sailing, Oscillating sail, Libration Point Orbits, Earth-Moon System, Orbit transfer

1. Introduction

The enabling potential of solar sailing in the Sun-Earth system has been extensively investigated and has resulted in a range of high-energy mission concepts such as missions over the poles of the Sun for heliophysics,[1)] hovering along the Sun-Earth line for space weather forecasting,[2)] and parking the sail above the Earth's orbit for high-latitude navigation and communication purposes.[3)] Instead, the potential of solar sailing in the *Earth-Moon* system has been investigated to a much lesser extent, while holding great promise for scientific and telecommunication capabilities due to the closer proximity to the Earth and Moon.

Previous work has established some of these capabilities by demonstrating the existence of families of solar sail periodic orbits in the Earth-Moon circular restricted three-body problem, mainly around the Earth[4)] and co-linear[5)] and triangular[6)] Lagrange points. For example, in 4) the authors demonstrate the use of solar sail Earth-centered periodic orbits for high-latitude observation of the Earth and solar sail vertical Lyapunov orbits at the Earth-Moon L_2-point for continuous coverage of the Aitken Basin and South Pole of the Moon for observation and telecommunication purposes during future human exploration missions to the far-side of the Moon.

This paper considers similar capabilities by exploiting the concept of an oscillating sail,[7)] which consists of using a solar sail that oscillates around the Sun-line when released at an initially deflected angle. This oscillating motion is created through a centre-of-mass/centre-of-pressure offset and can be exploited to achieve novel mission concepts. For example, the work in 7) has demonstrated that, by synchronizing the sail attitude with the orbital period, orbit raising around the Earth can be achieved.

As this paper will demonstrate, combining the novel concept of the oscillating solar sail with the dynamics of the Earth-Moon system results in additional, new families of solar sail periodic orbits. These orbits are obtained through a differential correction scheme in combination with a continuation approach to give rise to families of periodic orbits that are parameterised by the sail performance. While this paper will focus only on planar orbits (including solar sail Lyapunov and distant retrograde orbits), the extension to the three-dimensional case is straightforward, as already demonstrated for the use of traditional solar sails in 5).

Finally, in addition to using the solar sail to alter the shape of classical periodic orbits in the Earth-Moon three-body problem, this paper also investigates its use for transferring *between* classical periodic orbits. By using a systematic search approach in combination with a local optimisation method, the oscillating sail parameters that allow transfers between different orbits of the same classical L_1-Lyapunov orbit family or classical distant retrograde orbit (DRO) family can be established as well as transfers between classical Lyapunov orbits at different

Lagrange points. By deploying the oscillating sail when the transfer needs to be initiated and ejecting or re-folding the sail upon arrival in the targeted classical libration point orbit, the oscillating sail provides an efficient form of propulsion to transfer within the Earth-Moon system.

2. Dynamical System

In this paper, solar sail periodic orbits in the Earth-Moon system are developed within the framework of the circular restricted three-body problem (CR3BP). The equations of motion that describe the solar sail dynamics in the CR3BP are well-known and are given as[8)]

$$\ddot{\mathbf{r}} + 2\boldsymbol{\omega} \times \dot{\mathbf{r}} = \mathbf{a}_s(t) - \nabla U \,. \tag{1}$$

In Eq. (1), $\mathbf{r} = \begin{bmatrix} x & y & z \end{bmatrix}^T$ is the solar sail position vector in the Earth-Moon synodic reference frame of Fig. 1a. Furthermore, the dot indicates the derivative with respect to time and $\boldsymbol{\omega} = \omega \hat{\mathbf{z}}$ with ω the angular velocity of the two bodies around their common center-of-mass (i.e., the angular velocity of the synodic reference frame).

The right-hand side of Eq. (1) includes the solar sail induced acceleration, $\mathbf{a}_s(t)$, and the effective potential

$$U = -\tfrac{1}{2}\left(x^2 + y^2\right) - \left(\left[1-\mu\right]/r_1 + \mu/r_2\right) \tag{2}$$

with $\mu = m_2/(m_1+m_2) = 0.01215$, $\mathbf{r}_1 = \begin{bmatrix} x-\mu & y & x \end{bmatrix}^T$ and $\mathbf{r}_2 = \begin{bmatrix} x-(1-\mu) & y & x \end{bmatrix}^T$, see also Fig. 1a.

To define the solar sail acceleration, an ideal solar sail model is assumed, which considers the sail to be a perfect reflector without wrinkles or other optical imperfections.[8)] Under these assumptions, the sail reflects the solar photons specularly and the acceleration acts perpendicular to the solar sail membrane, in direction $\hat{\mathbf{n}}$. Furthermore, it is assumed that the solar radiation pressure is constant throughout the Earth-Moon system, resulting in

$$\mathbf{a}_s(t) = a_c \left(\hat{\mathbf{S}}(t) \cdot \hat{\mathbf{n}}\right)^2 \hat{\mathbf{n}} \tag{3}$$

with $\hat{\mathbf{S}}$ the direction of Sunlight (see Fig. 1b) and a_c the dimensionless characteristic solar sail acceleration. Note that, for the initial investigations in this paper, the Sun is assumed to orbit in the Earth-Moon plane, neglecting the small (5.1 deg) offset between the ecliptic and Earth-Moon planes, resulting in

$$\hat{\mathbf{S}}(t) = \begin{bmatrix} \cos(\Omega_S t) & -\sin(\Omega_S t) & 0 \end{bmatrix}^T \tag{4}$$

where $\Omega_S = 0.9252$ is the angular rate of the Sun around the Earth-Moon system, again see Fig. 1b. The dot product between the direction of Sunlight and the solar sail normal vector in Eq. (3) can also be written as the cosine of the cone angle, α, which equals the angle between the Sun-direction and the direction of the acceleration vector (i.e., $\hat{\mathbf{n}}$):

$$\mathbf{a}_s(t) = a_c \cos\alpha^2 \hat{\mathbf{n}} \,. \tag{5}$$

Note that a set of canonical units is used in the dynamics of Eqs. (1)-(5), whereby the sum of the two larger masses, the distance between the main bodies, and $1/\omega$ are taken as the unit of mass, length and time, respectively. In dimensional form (indicated by the tilde) the characteristic acceleration at the Earth-Moon system's solar distance of 1 Astronomical Unit (AU) is given by

$$\tilde{a}_c = \beta \frac{\mu_S}{\mathrm{AU}^2} \tag{6}$$

with μ_S the gravitational parameter of the Sun and β the solar sail lightness number. The lightness number is a function of the ratio of the solar sail area and the spacecraft mass and increases for increasing sail performances. Previous solar sail missions have achieved lightness numbers of $\beta = 0.001$ (IKAROS (JAXA, 2010)),[9)] $\beta = 0.003$ (NanoSail-D2 (NASA, 2010))[10)] and $\beta = 0.011$ (LightSail-1 (Planetary Society, 2015))[11)]. A similar lightness number value to that of LightSail-1 is expected for NASA's proposed NEA Scout mission, $\beta = 0.01$,[12)] while NASA's previously proposed Sunjammer mission would have achieved a lightness number of $\beta = 0.0363$.[2)] The latter corresponds to a dimensionless characteristic acceleration of $a_c = 0.0798$ and therefore a maximum value of $a_c = 0.1$ will be considered in this paper.

a)

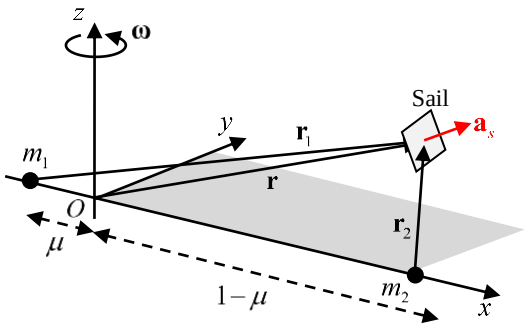

b)

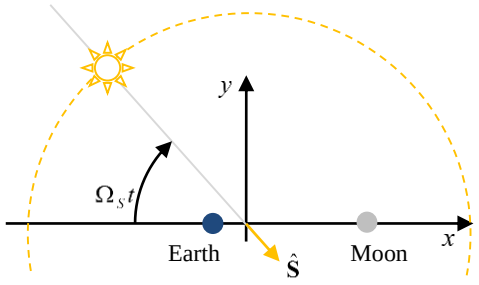

Fig. 1 a) Schematic of solar sail circular restricted three-body problem. b) Schematic of non-autonomous solar sail Earth-Moon three-body problem.

3. Oscillating solar sail

From Eq. (3) it is clear that the solar sail acceleration vector depends on the solar sail attitude, which is described through the normal to the solar sail membrane, $\hat{\mathbf{n}}$. Therefore, by considering different solar sail steering laws, different families of solar sail periodic orbits and transfers between orbits will originate. This document considers the concept of an oscillating solar sail,[7)] which involves a sail attached to a spacecraft bus that conducts an oscillating motion around the Sun-line with an

oscillation amplitude of θ_0, see Fig. 2. The variation of the deflection angle over time can then be written as[13)]

$$\theta(t) = \theta_0 \sin\left(\frac{2\pi}{T_{osc}} t + \phi_{osc}\right) \tag{7}$$

with T_{osc} and ϕ_{osc} the period and phase of the oscillation. The variation of the cone angle over time then follows from

$$\alpha(t) = 90° - |\theta(t)| . \tag{8}$$

Furthermore, the solar sail normal vector with respect to an auxiliary reference frame $(\hat{\mathbf{s}}, \hat{\mathbf{l}}, \hat{\mathbf{p}})$, see Fig. 2, can be defined as:

$$\hat{\mathbf{n}}|_{(\hat{\mathbf{s}},\hat{\mathbf{l}},\hat{\mathbf{p}})} = \begin{bmatrix} \cos\alpha & -\text{sign}(\theta)\sin\alpha & 0 \end{bmatrix}^T . \tag{9}$$

Finally, a rotation around the $\hat{\mathbf{p}}$ - axis will provide the solar sail normal vector with respect to the synodic reference frame of Fig. 1a for substitution into Eq. (3) or (5):

$$\hat{\mathbf{n}} = R_z(-\Omega_S t)\hat{\mathbf{n}}|_{(\hat{\mathbf{s}},\hat{\mathbf{l}},\hat{\mathbf{p}})} . \tag{10}$$

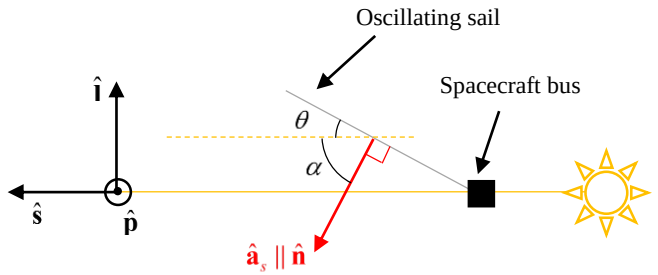

Fig. 2 Schematic of oscillating solar sail and auxiliary reference frame $(\hat{\mathbf{s}}, \hat{\mathbf{l}}, \hat{\mathbf{p}})$.

4. Differential corrector

In order to find oscillating sail periodic orbits in the Earth-Moon system, a differential correction scheme is applied, which iteratively finds the initial conditions that allow for periodic orbits. This differential correction scheme largely follows the method introduced by Howell in 14), but introduces a constraint to drive the orbital period to one synodic lunar period or a multiple thereof. The synodic lunar period is the period of the Sun around the Earth-Moon system, i.e., $2\pi / \Omega_S$, and this constraint is required to ensure that the Sun-sail-Earth/Moon system configuration is the same at the start and end of the orbit so that the solar sail orbit is repeatable over time. More details on the differential corrector method can be found in 5).

To seed the differential corrector, classical periodic orbits are used that have a suitable period, i.e., a period equal to a fraction (or multiple) of the synodic lunar period. A continuation method is subsequently applied, whereby the solar sail characteristic acceleration, a_c, is slowly increased, using the result for a slightly smaller sail acceleration as initial guess to start the differential corrector for a slightly larger sail acceleration. This approach will give rise to families of periodic orbits for increasing sail performance. Note that the continuation scheme is truncated when the differential corrector scheme does not converge for a minimum step size of $\Delta a_c = 10^{-7}$ within 100 iterations.

As examples of initial guesses, Fig. 3 shows the families of classical L_1-Lyapunov orbits (Fig. 3a) and DROs (Fig. 3b) together with their orbital period as a function of their initial x-coordinate. The orbits with suitable periods (i.e., a fraction of the synodic lunar month) are indicated with coloured lines in the orbital plots and with a coloured marker in the plot showing the orbits' period. Note that two orbits of the DRO family can serve as an initial guess: one with a period of half the synodic lunar month (hereafter referred to as $DRO_{1/2}$) and one with a period equal to a third of the synodic lunar month (hereafter referred to as $DRO_{1/3}$). Therefore, two and three revolutions (respectively) in these orbits will serve as initial guess for the differential corrector in order to fulfill the requirement that the solar sail orbits should have an orbital period equal to one synodic lunar month (or a multiple thereof).

From the classical libration point orbits in Fig. 3 it becomes clear that the orbits cross the (x,z)-plane twice. The left-hand side crossings are used to produce the orbital period plots in Fig. 3. However the other (x,z)-plane crossing (to the right of the L_1-point/Moon) could also be considered as initial condition and will result in different Sun-sail configurations along the orbit and therefore in different orbit families.[4, 5)] However, for brevity, this paper will only consider the left-hand side crossing.

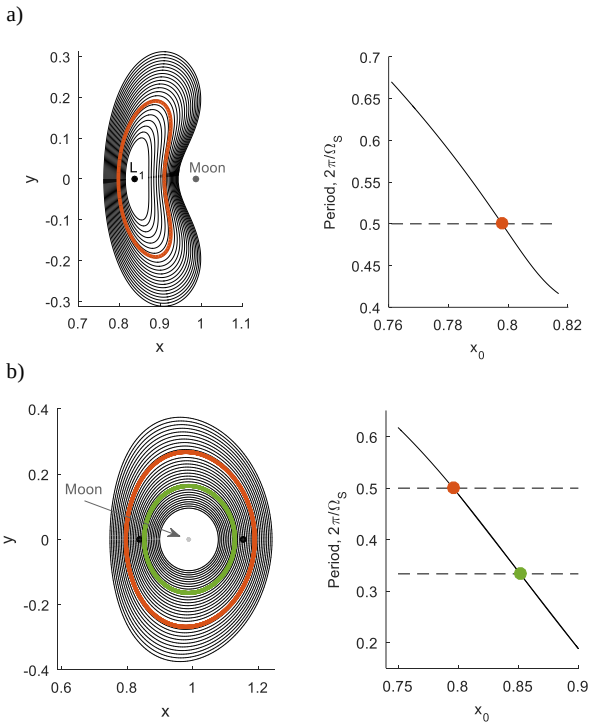

Fig. 3 Classical libration point orbits and their orbital periods. A) Family of Lyapunov orbits at the L_1-point. b) Family of DROs.

5. Oscillating sail periodic orbits

This paper provides results for a range of families of oscillating solar sail periodic orbits in the Earth-Moon system. The results presented are all obtained for $T_{osc} = 2\pi / \Omega_S$ and $\phi_{osc} = 0$, indicating that the oscillating motion and period of the Sun around the Earth-Moon system are commensurable and that the sail starts at a zero-deflection state at time $t = 0$, i.e.,

$\theta(t) = \theta(0) = 0$. Initial analyses on the effect of the value for these parameters will be presented in Section 5.3. Note that a value for the oscillation phase of $\phi_{osc} = 0$ is chosen to create a symmetric acceleration profile during the synodic lunar period and that it will require the sail to be released with a non-zero angular velocity in order for it to obtain an oscillation between $\pm\theta_0$. Only for $\phi_{osc} = \pm 1/2\pi$, i.e., $\theta(0) = \theta_0$, can the sail be released with zero angular velocity while still obtaining the desired oscillatory motion.

5.1 Family of oscillating sail Lyapunov orbits

The results for the family of solar sail Lyapunov orbits at the L_1- and L_2-points are provided in Fig. 4a. Colours indicate the dimensionless solar sail characteristic acceleration whereas crosses indicate the initial conditions. To compare the results with previously obtained results[5] for a traditional, Sun-facing sail (i.e., $\hat{\mathbf{n}} = \hat{\mathbf{S}}$) where the sail's membrane is always fully exposed to the Sun, Fig. 4b is included. Fig. 4b shows very similar results to those obtained for the oscillating sail at the L_1-point, but significant differences can be observed at the L_2-point where the Sun-facing steering law resulted in a premature truncation of the orbit family, while a full family exists for the oscillating sail.

Other differences between the two steering laws may exist in, for example, the stability of the orbits. An example of this is given in Fig. 4c, which provides details on the linear stability of the orbits at the L_1-point. The figure shows the maximum norm of the eigenvalues of the monodromy matrix, which is the state transition matrix evaluated after one full orbit, i.e., at time $t = 2\pi / \Omega_S$. An orbit is stable if all six eigenvalues lie on the unit circle, i.e., $\|\lambda\|_{\max} = 1$. If the norm of any of the eigenvalues is larger than one, the orbit is unstable, with larger norm values indicating greater instability. The results in Fig. 4c show that the solar sail Lyapunov orbits are very unstable, but that the oscillating sail allows for slightly more stable orbits than the Sun-facing steering law.

5.2 Family of oscillating DROs

Additional orbit families, of oscillating solar sail DROs, are provided in Fig. 5a (for $DRO_{1/2}$) and Fig. 5b (for $DRO_{1/3}$). The orbits presented in Fig. 5a and b are very similar to the ones found with a Sun-facing steering law in 5), but their linear stability is rather different. This stability is provided in Fig. 5c for $DRO_{1/2}$. The figure shows that, especially for larger values for the solar sail characteristic acceleration, the oscillating sail can have a positive effect on the orbit stability.

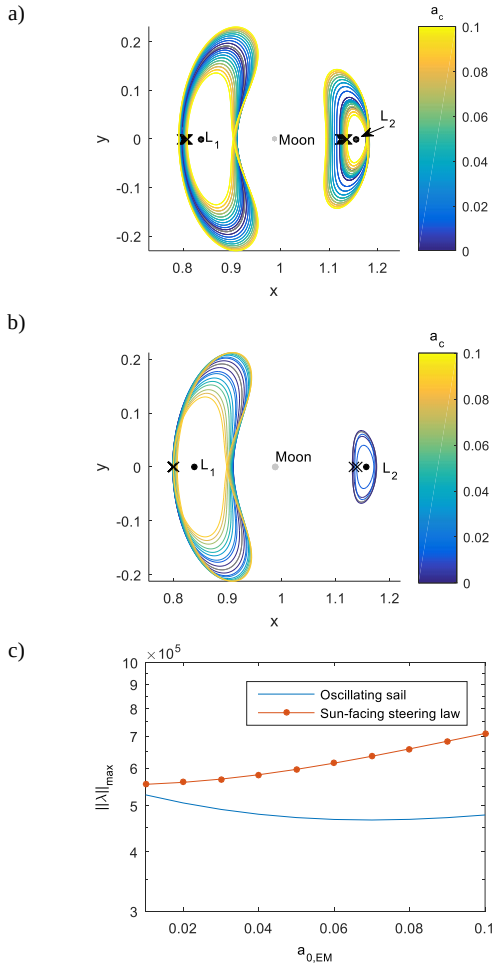

Fig. 4 Solar sail Lyapunov orbits at L_1 and L_2 for different values of the dimensionless characteristic acceleration, a_c. The grey orbit is the classical Lyapunov orbit to seed the differential corrector and crosses indicate the initial condition. a) For an oscillating sail. b) For a Sun-facing steering law. c) Linear stability.

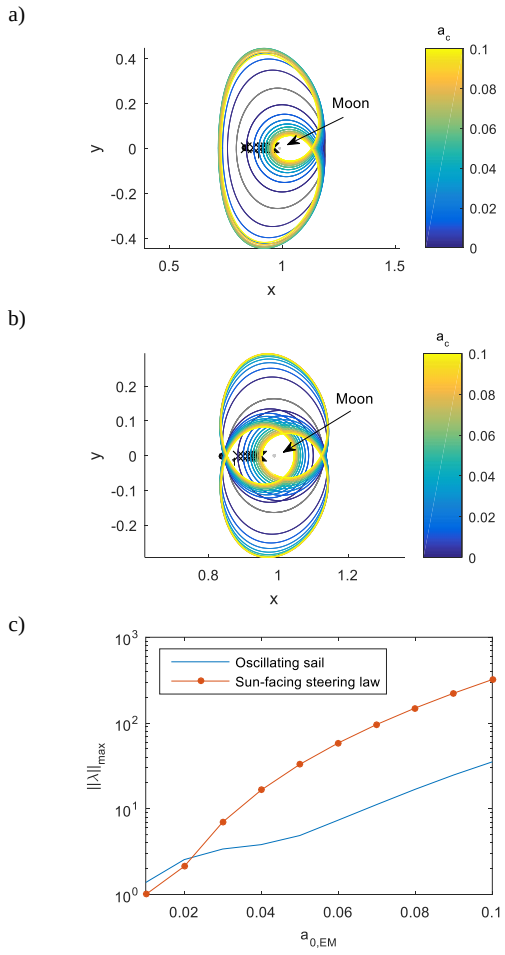

Fig. 5 Oscillating sail DROs for different values of the dimensionless characteristic acceleration, a_c. The grey orbit is the classical DRO to seed the differential corrector and crosses indicate the initial condition. a) For $DRO_{1/2}$. b) For $DRO_{1/3}$. c) Linear stability for $DRO_{1/2}$.

5.3 Effect of oscillating amplitude, period, and phase

The results so far have all been generated assuming an oscillating amplitude of 90 deg, an oscillation period of one synodic lunar month and a zero-oscillation phase ($\theta_0 = 90$ deg, $T_{osc} = 2\pi / \Omega_S$, and $\phi_{osc} = 0$). In this section, analyses on the effect of the values for these parameters are conducted for the L_1-Lyapunov orbit and $DRO_{1/2}$ with $a_c = 0.1$. Regarding the oscillating amplitude, Fig. 6a provides its effect by considering a range of values between 10 and 90 deg. The effect on the orbit is provided in the figures on the left, whereas the figures on the right show the maximum value for the y -coordinate as an indication of the achieved displacement. These latter figures show that the maximum displacement is not achieved for $\theta_0 =$ 90 deg, but for a smaller value ($\theta_0 = 70$ deg and $\theta_0 = 50$ deg for the Lyapunov orbits and DROs, respectively). The effect of the oscillation period is demonstrated in Fig. 6b by considering different fractions of the synodic lunar period as oscillation period. The figure shows that the oscillation period has some effect, but does not significantly change the shape of the solar sail orbit. A similar conclusion can be drawn for the effect of the oscillation phase in Fig. 6c. Note that only limited values for the oscillation phase can be assumed because symmetry in the control profile needs to be maintained: the second half of the orbit must be an exact mirror image (both in terms of state- and control-profiles) of the first half of the orbit in order for the differential correction scheme to produce *periodic* orbits. Therefore, $\phi_{osc} = 90$ deg does not result in periodic orbits, while $\phi_{osc} = 180$ deg does.

6. Oscillating sail orbital transfers

Rather than using the oscillating sail to alter the shape of the classical periodic orbits, the sail can potentially also be used to transfer between orbits. Here, the idea is that the satellite is initially injected into a *classical* libration point orbit. Subsequently, after the mission objectives in this orbit have been fulfilled, the oscillating sail is deployed to transfer the satellite to a larger/smaller classical libration point orbit or to a classical orbit at a different Lagrange point. Upon arrival in the new orbit, the sail is ejected or re-folded for future use.

The possibility to use the oscillating sail for this purpose will once again be demonstrated for transfers between Lyapunov orbits and distant retrograde orbits. Furthermore, it is assumed that the transfer starts from the classical orbits that have previously been selected to serve as a suitable initial guess for the solar sail periodic orbits, see Fig. 3.

6.1 Systematic search

To get a first idea whether the oscillating sail would be able to achieve such transfers, its dynamics have been integrated for a large range of sail and trajectory parameters. This integration starts from the left-hand-side (x,z) -plane crossing of the classical orbits in Fig. 3 and is truncated at one of the subsequent (x,z) -plane crossings. Subsequently, the state vector at the end of these trajectories is compared to the initial conditions of the families of classical Lyapunov orbits or DROs and if any of these coincide, a possible transfer may be found.

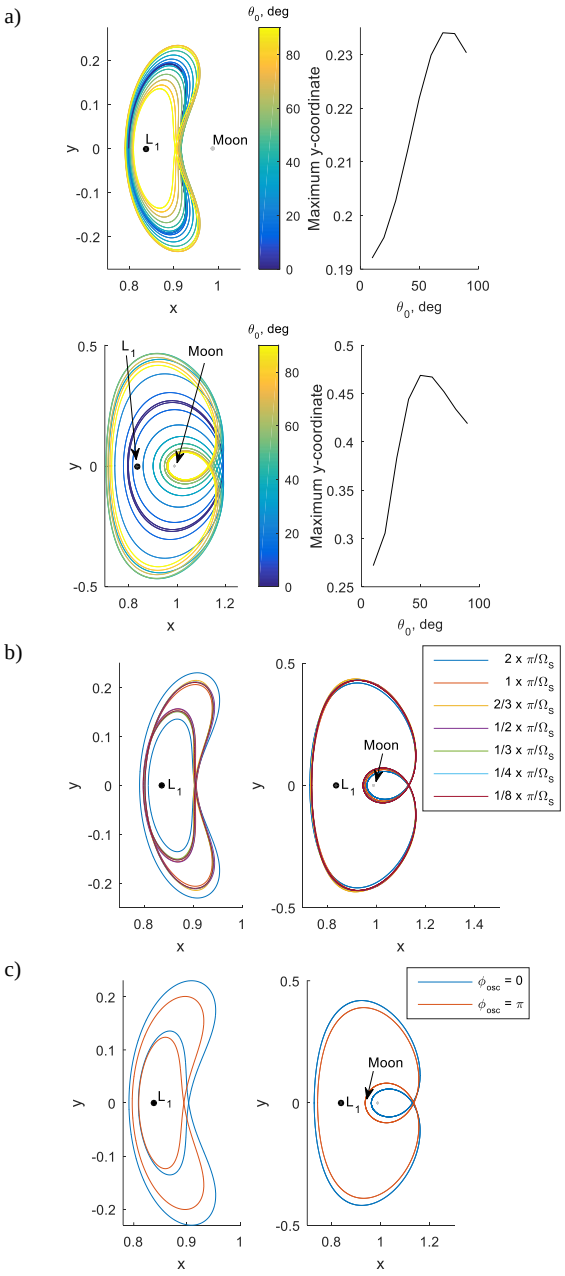

Fig. 6 Effect of oscillation amplitude (subplot a)), oscillation period (subplot b)) and phase (subplot c)) on L_1-Lyapunov orbit and $DRO_{1/2}$ for a_c= 0.1.

This concept is further illustrated in Fig. 7a and b: the black dots and stars indicate the x -position and velocity in y -direction of the family of *classical* Lyapunov orbits at L_1 at their intersections with the (x,z) -plane (dots and stars are used to distinguish between the (x,z) -plane crossings on the Earth and lunar sides of the L_1-point, respectively). Furthermore, the red dot in Fig. 7a indicates the states of the Earth-side (x,z) -plane crossing of the Lyapunov orbit in Fig. 7a, which is used as initial condition of the oscillating sail transfer. Finally, the remaining coloured dots indicate similar states, but at the end of the integrated oscillating sail trajectories. Note that not all integrated oscillating sail trajectories are included in this figure; only those with a near-zero velocity in x -direction upon the final (x,z) -plane crossing, $v_{x,f} \approx 0$, are shown.

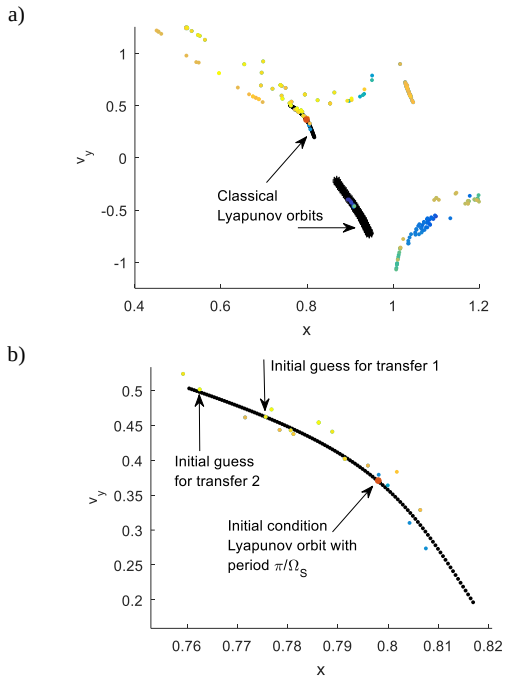

Fig. 7 Black dots and stars indicate the *x*-position and velocity in *y*-direction of the classical Lyapunov orbits at L_1 at their (*x*,*z*)-plane crossings. Coloured dots indicate these states at the end of oscillating sail trajectories that satisfy $v_{x,f} \approx 0$. Subplot b) is a detail of subplot a).

The actual colour of the dots indicates the particular set of sail parameters considered. In particular, the following parameters and range in their values have been implemented in the systematic search:

- Oscillation amplitude, θ_0, in the range: $\theta_0 \in \left[40^o, 90^o\right]$ with a step-size of $\Delta\theta_0 = 10^o$.
- Oscillation period, T_{osc}, with values: $T_{osc} = \frac{\pi}{\Omega_S}\left[\frac{1}{4},\ \frac{1}{3},\ \frac{1}{2},\ \frac{2}{3},\ \frac{3}{4},\ 1,\ \frac{3}{2},\ 2\right]$
- Oscillation phases, ϕ_{osc}, in the range: $\phi_{osc} \in \left[0^o, 360^o\right]$ with a step-size of $\Delta\phi_{osc} = 30^o$
- Dimensionless sail characteristic accelerations, a_c, in the range: $a_c \in \left[0, 0.5\right]$ with a step-size of $\Delta a_c = 0.0005$
- Transfer times, which are expressed as the number of allowed (x,z)-plane crossings before the integration is truncated: 1, 2, 3, 4, or 5

The results in Fig. 7 suggest that a few of these cases provide trajectories where the end state (nearly) coincides with the initial conditions of the family of L_1-Lyapunov orbits. Dots that remain close to the red dot in Fig. 7b represent oscillating sail trajectories that remain close to the classical L_1-Lyapunov orbit of Fig. 3a. However, coloured dots that lie further down/up the Lyapunov family indicate the possibility for a transfer to a larger/smaller Lyapunov orbit.

The trajectory for the dot indicated with 'Initial guess for transfer 1' is provided in Fig. 8 and its parameters are provided in the first data-column of Table 1. The figure shows the initial classical orbit (i.e., the orbit in Fig. 3a) as a red dotted line and the transfer as a black solid line. The *classical* dynamics (i.e., without the oscillating sail) are continued at the end of the transfer to see if the satellite indeed ended up in a larger Lyapunov orbit. However, the figure clearly shows that the dynamics divert from a Lyapunov-shaped orbit after half an orbit revolution. Some divergence can be expected because Lyapunov orbits are very unstable (see the linear stability values in Fig. 4c): a small error in the initial conditions (or even in the integration method or tolerance) can result in very different trajectories. It is therefore expected that some form of control will be required to maintain these classical orbits as is the case for current ballistic libration point missions. However, tweaking of the oscillating sail parameters can be conducted to improve the initial guess in Fig. 8.

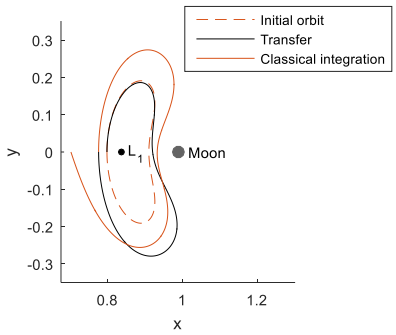

Fig. 8 Initial guess for transfer 1 between two L_1-Lyapunov orbits.

6.2 Local optimisation

The systematic search over the oscillating sail and trajectory parameters in the previous sub-section has provided some good guesses for potential transfers between libration point orbits. In this section, a further tweaking of these parameters is performed to truly match the Lyapunov orbit conditions at the end of the transfer. For this, a local optimisation algorithm, implemented in MATLAB's *fmincon.m* function is used. The decision variables are those used for the systematic search, i.e., θ_0, T_{osc}, ϕ_{osc}, and a_c. However, note that the "transfer time" (i.e, the number of allowed (x,z)-plane crossing before the integration is truncated) is the same as found for the initial guess. Bounds on the values for these decision variables are set to ±10% of the values provided by the initial guess, although in some cases the bound on a single decision variable has been further decreased/increased if initial optimisations indicated that the solution was close to its lower or upper bound.

A two-stage optimisation process is employed, using two different sets of objective functions and non-linear constraints:

1. The objective of the first optimisation is to minimise the difference in state-vector between the end of the transfer and *any* of the initial conditions of the orbits in the Lyapunov and DRO family. No non-linear constraints are applied in this case. The result of this optimisation is used as initial guess for the second stage.
2. In the second stage, the objective of the optimisation is set to zero and the following set of non-linear constraints is applied to the ***integrated classical dynamics following the transfer*** (i.e., to the solid red line in Fig. 8):

$$\begin{aligned} \tilde{v}_{x,0} &= 0 \\ \tilde{v}_{x,f} &= 0 \\ \tilde{\mathbf{x}}_0 &= \tilde{\mathbf{x}}_f \end{aligned} \qquad (11)$$

The first two constraints require the velocity in x-direction at the start and end of the solid red line in Fig. 8 to be zero, while the third constraint requires the initial and final state vectors of this trajectory to be the same. Note that the second constraint is implied by the third constraint, but better performance of the optimiser was obtained with the addition of the second constraint.

The required accuracy of the optimised transfer is such that integration of the conditions at the end of the transfer, i.e., $\tilde{\mathbf{x}}_0$, allow for *at least* two revolutions in the final classical Lyapunov orbit before slight divergence from this orbit starts to occur.

6.3 Results

6.3.1 Transfer between classical L_1-Lyapunov orbits

The result of the local optimisation of the transfer in Fig. 8 is provided in Fig. 9a and the second data-column in Table 1. An additional transfer, indicated by the dot in Fig. 7b labeled as "Initial guess for transfer 2" is also shown in Fig. 9b with the initial guess data and optimised data in Table 1. Both transfers show the feasibility of using a near-term solar sail ($a_c < 0.1$) to transfer between different sized classical L_1-Lyapunov orbits. The Jacobi constant of the initial orbit is 3.0663 for both transfers, but the Jacobi constants of the final orbits are 3.0286 and 2.9797, indicating that energy has been added to the satellite during the oscillating sail transfer.

6.3.2 Transfer between classical Lyapunov orbits at different Lagrange points

While the analysis of the results in Fig. 7a focused on the overlap between the L_1-Lyapunov family and the oscillating sail transfers, it only shows part of the feasible trajectories: the plot in Fig. 7a is a close-up, while Fig. 10a provides the full overview. Fig. 10a not only includes the conditions at the (x,z)-plane crossings of the Lyapunov family at L_1, but also those conditions for the Lyapunov families at L_2 and L_3. The figure shows that some coloured dots coincide with the orbits at L_2 and L_3, suggesting the existence of transfers between Lyapunov orbits at L_1 and L_2/L_3. Therefore, details of Fig. 10a in close vicinity of the L_3-and L_2-families are provided in Fig. 10b and c, respectively. These figures also show which dots are selected as an initial guess for the local optimisation. Details of these initial guesses and the optimised results can be found in Fig. 11 and Table 1. Interesting to note is that the Jacobi constants of the final Lyapunov orbits for "transfer 3" and "transfer 4" are 2.9684 and 3.0672, respectively. Considering that the Jacobi constant of the initial orbit is still 3.0663, these values show that energy has been added to the system during "transfer 3", but energy has been extracted from the system during "transfer 4".

While "transfer 3" to the L_3-point is perfectly feasible with near-term sail technology, this is not true for "transfer 4" to the L_2-point. This transfer requires a sail performance ($a_c = 0.4498$) that is approximately 5 times higher than near-term sail technology. In addition, the transfer dips just below the lunar surface, making this transfer infeasible. Other, *feasible* trajectories between the L_1- and L_2-point have so far not been found, but the search for such a transfer will be part of future work.

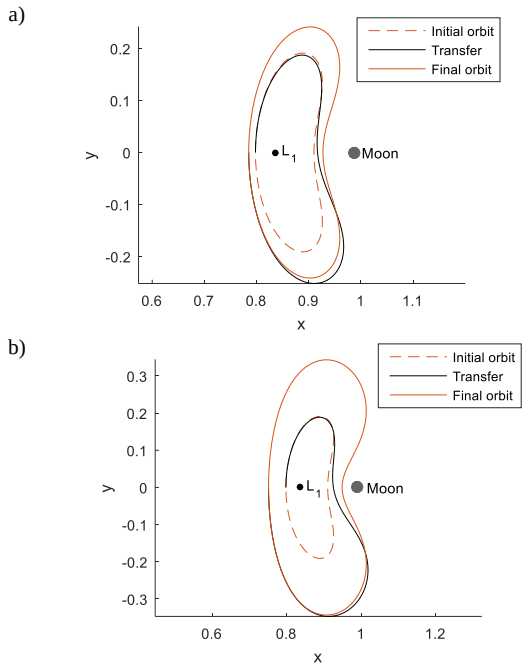

Fig. 9 Optimised oscillating sail transfer between classical L_1-Lypapunov orbits. a) "Transfer 1". b) "Transfer 2".

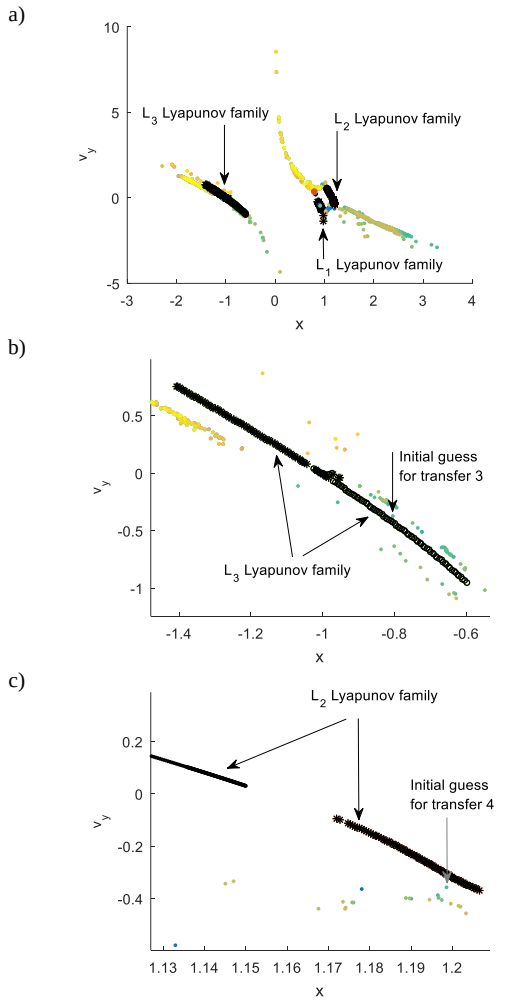

Fig. 10 Black dots and stars indicate the x-position and velocity in y-direction of classical Lyapunov orbits at any of the three co-linear Lagrange points at their (x,z)-plane crossings. Coloured dots indicate these states at the end of oscillating sail trajectories that satisfy $v_{x,f} \approx 0$.

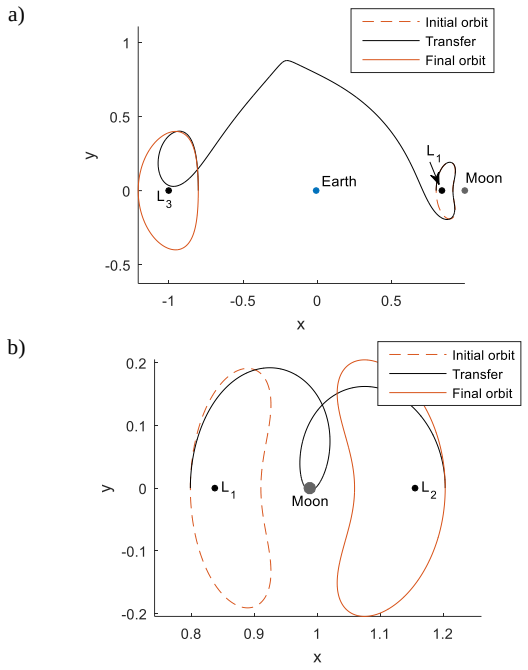

Fig. 11 Optimised oscillating sail transfer between classical L_1-Lypapunov orbits and L_2- and L_3-Lyapunov orbits. a) "Transfer 3". b) "Transfer 4".

6.3.3 Transfers between classical DROs

The same approach and algorithm applied to the search for oscillating sail transfers between Lyapunov orbits can also be applied to finding transfers between distant retrograde orbits. In Fig. 3b two classical DROs were identified that have suitable periods to find solar sail periodic orbits in the Earth-Moon system. Starting from these two orbits ($DRO_{1/2}$ and $DRO_{1/3}$), the results as presented in Fig. 12, Fig. 13 and Table 1 are obtained. These transfers once again show that the oscillating sail can be used successfully to transfer between classical periodic orbits using near- to mid-term sail technology. In both cases the Jacobi constant of the final orbit is smaller than that of the initial orbit, indicating that energy has been added to the system during the transfer.

7. System analysis

The sail characteristic acceleration is directly related to the system loading $\sigma = m/A$, where m is the total mass of the spacecraft and A the area of the sail. Considering that $a_c = 2AP_{sun}\eta/m$, we obtain $\sigma = 2P_{sun}\eta/a_c$ where $P_{sun} = 4.56\times10^{-6}$ Pa is the solar radiation pressure at 1 AU (considered constant in this work), and $\eta = 0.85$ is a parameter to take into account the non-ideal reflectivity of the sail (within the specular reflectivity assumption). The system loading, as a_c, gives an idea of the technological requirements of the sail. Assuming that the mass of the spacecraft bus is negligible with respect to that of the sail assembly, then σ becomes an indicator of the areal density of the sail itself (or sail loading). Considering a traditional square sail, of side l, its mass is $m = \sigma l^2$ and its moment of inertia, with respect to the oscillation axis and translated into the centre of mass, is $I = \left(l^4/12 + l^2 d^2\right)\sigma$. Here, d is the distance between the centre of mass and the geometric centre, which coincides with the centre of pressure of the sail, or static margin.

According to 7), the oscillation period can be computed as:

$$T = 4\sqrt{\frac{I}{2\eta P_s A d\cos^2(\delta_s)}}\int_0^{\theta_0}\frac{d\theta}{\sqrt{\theta_0 - \frac{1}{2}\sin 2\theta_0 - \theta + \frac{1}{2}\sin 2\theta}} \qquad (12)$$

where the declination of the Sun equals $\delta_s = 0$ because the

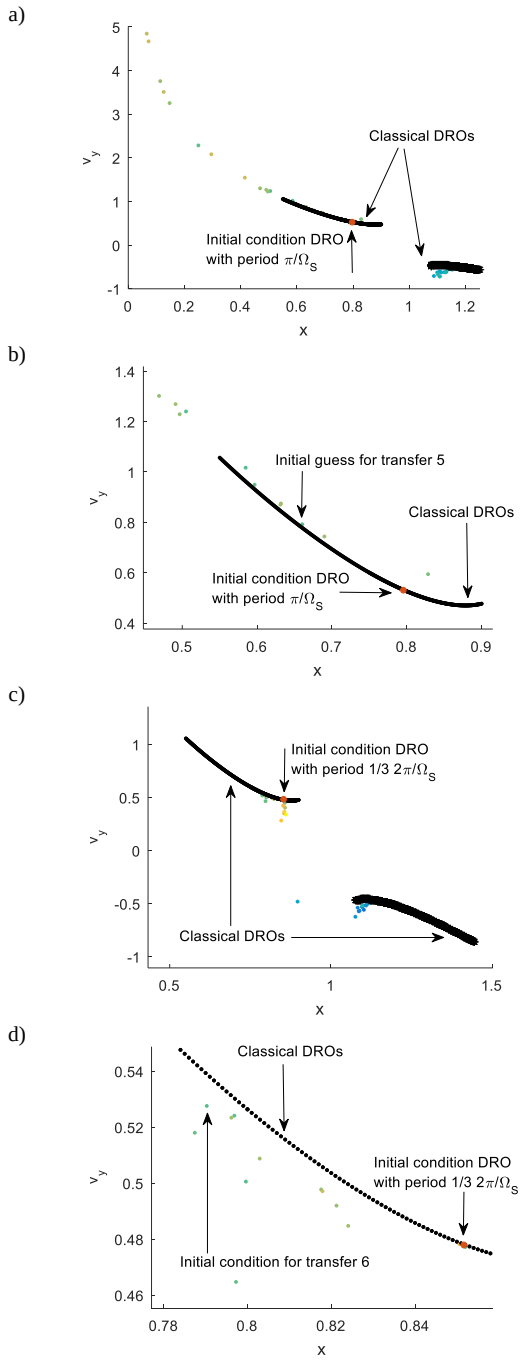

Fig. 12 Black dots and stars indicate the x-position and velocity in y-direction of the classical DROs at their (x,z)-plane intersections. Coloured dots indicate these states at the end of oscillating sail trajectories that satisfy $v_{x,f} \approx 0$. Subplot b) and d) are details of subplots a) and c), respectively. Subplots a-b) and c-d) are for transfers starting from $DRO_{1/2}$ and $DRO_{1/3}$, respectively.

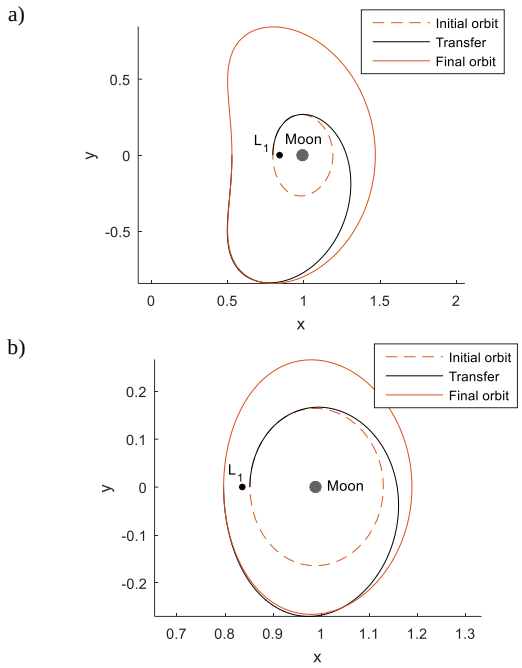

Fig. 13 Optimised oscillating sail transfer between classical DROs. a) "Transfer 5". b) "Transfer 6".

Sun is assumed in the plane of the sail oscillation, and θ_0 is the oscillation amplitude, as required by the orbits and transfers computed in the previous sections.

Assuming, for example, a sail with $l = 100$ m, Fig. 14 shows the period as a function of the static margin d: in subplot a) for the range of oscillating amplitudes and oscillating periods used in Fig. 6a and b (the horizontal dotted black lines correspond to the oscillating periods in Fig. 6b) and in subplot b) for each of the transfer cases presented in Section 6. Note that for the results in Fig. 14b the equation can be inverted to find d, for a given required oscillation period, and the result is represented with a circle for each one of the transfer cases. As a general result for all orbits and transfers, we note that in order to achieve the relatively long oscillation periods, the static margin must be considerably small, of the order of cm to a fraction of a mm. This implies that either extreme accuracy is required in manufacturing of the spacecraft and deployment of the sail, or a small vane or reflectivity control device is needed to accurately position the center of pressure within the sail.

8. Conclusions

This paper has exploited the concept of an oscillating sail to create new families of solar sail periodic orbits in the Earth-Moon system, parameterised by the sail performance, as well as transfers between classical periodic orbits. In particular, families of, and transfers between, planar, solar sail Lyapunov orbits and distant retrograde orbits have been considered. The newly created families of oscillating sail orbits have been shown to be very similar to those obtained with a traditional, Sun-facing solar sail, but in some cases allow the family to continue to larger values for the sail's characteristic acceleration and show more advantageous linear stability properties. Regarding the transfers, the capability of the oscillating sail to transfer between classical orbits that belong to the same L_1-Lyapunov family or DRO family as well as transfers between Lyapunov orbits at different Lagrange points has been demonstrated. While in most cases the oscillating sail is used to add energy to the system (e.g., to move from a small-amplitude to a larger-amplitude Lyapunov orbit or DRO), it can also be used to extract energy from the system (e.g., to move between two particular Lyapunov orbits at the L_1-and L_2-points).

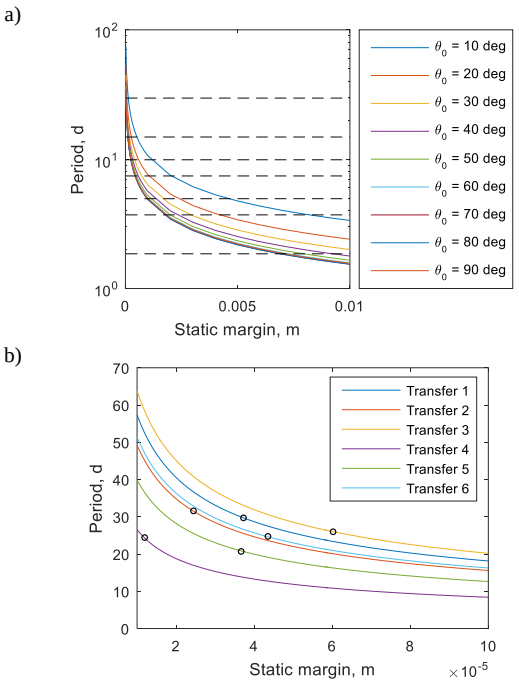

Fig. 14 Oscillation period varying the static margin, for a square 100 × 100 m^2 sail. a) For a range of oscillating amplitudes and oscillating periods. b) For the optimised transfers. Circles represent the design points for achieving the required period on each transfer.

Acknowledgments

Jeannette Heiligers acknowledges the support of the Marie Skłodowska-Curie Individual Fellowship 658645 - S4ILS: Solar Sailing for Space Situational Awareness in the Lunar System.

References

1. Macdonald, M., Hughes, G.W., McInnes, C.R., Lyngvi, A., Falkner, P., and Atzei, A., "Solar Polar Orbiter: A Solar Sail Technology Reference Study," *Journal of Spacecraft and Rockets*; Vol. 43, No. 5, 2006, pp. 960-972. doi: 10.2514/1.16408
2. Heiligers, J., Diedrich, B., Derbes, B., and McInnes, C.R., "Sunjammer: Preliminary End-to-End Mission Design," *2014 AIAA/AAS Astrodynamics Specialist Conference*, San Diego, CA, USA, 2014.

3. Waters, T.J. and McInnes, C.R., "Periodic Orbits Above the Ecliptic in the Solar-Sail Restricted Three-Body Problem," *Journal of Guidance, Control, and Dynamics*; Vol. 30, No. 3, 2007, pp. 687-693. doi: 10.2514/1.26232
4. Heiligers, J., Parker, J.S., and Macdonald, M., "Novel Solar Sail Mission Concepts for High-Latitude Earth and Lunar Observation," *AIAA/AAS Astrodynamics Specialist Conference*, Long Beach, California, USA, 2016.
5. Heiligers, J., Macdonald, M., and Parker, J.S., "Extension of Earth-Moon Libration Point Orbits with Solar Sail Propulsion," *Astrophysics and Space Sciences, In Press*; Vol. 361 : 241, 2016. doi: 10.1007/s10509-016-2783-3
6. Jorba-Cuscó, M., Farrés, A., and Jorba, À., "Periodic and Quasi-Periodic Motion for a Solar Sail in the Earth-Moon System," *67th International Astronautical Congress*, Guadalajara, México, 2016.
7. Ceriotti, M., Harkness, P., and McRobb, M., "Synchronized Orbits and Oscillations for Free Attitude Control," *Journal of Guidance, Control, and Dynamics*; Vol. 37, No. 6, 2014, pp. 2062-2066. doi: 10.2514/1.G000253
8. McInnes, C.R., "Solar Sailing: Technology, Dynamics and Mission Applications," *Springer-Praxis Books in Astronautical Engineering*, Springer-Verlag, Berlin, 1999.
9. Tsuda, Y., Mori, O., Funase, R., Sawada, H., Yamamoto, T., Saiki, T., Endo, T., Yonekura, K., Hoshino, H., and Kawahuchi, J., "Achievement of IKAROS - Japanese deep space solar sail demonstration mission," *Acta Astronautica*; Vol. 82, 2013, pp. 183-188. doi: 10.1016/j.actaastro.2012.03.032
10. Johnson, L., Whorton, M., Heaton, A., Pinson, R., Laue, G., and Adams, C., "NanoSail-D: A Solar Sail Demonstration Mission," *Acta Astronautica*; Vol. 68, 2011, pp. 571-575. doi: 10.1016/j.actaastro.2010.02.008
11. Biddy, C. and Svitek, T., "LightSail-1 Solar Sail Design and Qualification," *Proceedings of the 41st Aerospace Mechanisms Symposium*, Pasadena, CA, 2012.
12. McNutt, L., Johnson, L., Clardy, D., Castillo-Rogez, J., Frick, A., and Jones, L., "Near-Earth Asteroid Scout," *AIAA SPACE 2014 Conference and Exposition*, American Institute of Aeronautics and Astronautics, San Diego, CA, 2014.
13. Ceriotti, M., "Unconventional Solar Sailing," *AstroNet-II International Final Conference*, Tossa de Mar, Spain, 2015.
14. Howell, K.C., "Three-dimensional, periodic, 'Halo' orbits," *Celestial Mechanics*; Vol. 32, 1983, pp. 53-71. doi: 10.1007/BF01358403

Table 1 Sail and trajectory parameters for transfers between classical Lyapunov orbits and DROs. *Note that transfer 4 is currently infeasible.

	Transfer 1		**Transfer 2**		**Transfer 3**		**Transfer 4***		**Transfer 5**		**Transfer 6**	
	Initial guess	**Opti-mised**	**Initial guess**	**Opti-mised**	**Initial guess**	**Opti-mised**	**Initial guess**	**Opti-mised**	**Initial guess**	**Opti-mised**	**Initial guess**	**Opti-mised**
Oscillation amplitude, deg	80	72.9	90	75.2	40	36.3	40	40.1	40	47.5	40	32.4
Oscillation period, days	29.67	29.73	29.67	31.51	29.67	26.00	22.25	24.30	22.25	20.84	22.25	24.66
Oscillation phase, deg	150	148.9	150	157.4	330	327.9	270	284.8	210	217.8	210	268.1
Sail characteristic acceleration, -	0.075	0.072	0.090	0.097	0.071	0.084	0.384	0.450	0.119	0.177	0.105	0.142
Multiplicity, number of (x,z)-plane crossings	1	1	1	1	4	4	2	2	1	1	1	1
Jacobi constant of initial classical orbit, -	-	3.0663	-	3.0663	-	3.0663	-	3.0663	-	2.9225	-	2.9623
Jacobi constant of final classical orbit, -	-	3.0286	-	2.9797	-	2.9683	-	3.0672	-	2.7346	-	2.9232
Required static margin for 100 x 100 m^2 sail, 10^{-5} m	-	3.720	-	2.443	-	6.020	-	1.193	-	3.666	-	4.344